Scientific Research Publishing

Open Journal of Applied Sciences, 2026, 16(4), 1246-1268
https://www.scirp.org/journal/ojapps
ISSN Online: 2165-3925
ISSN Print: 2165-3917

Modeling, Simulation, and Experimental Study of Landing Gear Shimmy Considering Strut Height Variation

Guisheng Zhu, Yanying Zhao*, Yian Liu, Zhenyuan Ju, Wenchong Feng

School of Aeronautics and Astronautics, Nanchang Hangkong University, Nanchang, China
Email: *yanyingzhao@nchu.edu.cn

How to cite this paper: Zhu, G.S., Zhao, Y.Y., Liu, Y., Ju, Z.Y. and Feng, W.C. (2026) Modeling, Simulation, and Experimental Study of Landing Gear Shimmy Considering Strut Height Variation. *Open Journal of Applied Sciences*, **16**, 1246-1268.
https://doi.org/10.4236/ojapps.2026.164072

Received: April 2, 2026
Accepted: April 25, 2026
Published: April 28, 2026

Abstract

In this paper, a four-degree-of-freedom dual-wheel nose landing gear shimmy dynamic model considering strut height variation is established for a certain aircraft nose landing gear. The reliability of the relationship between strut stiffness and strut height is verified by comparing the results of static simulation analysis with the theoretical model results. Then, using numerical analysis methods, the influence of strut height variation on the stable region and stability performance of the landing gear is analyzed. Through a taxiing simulation test bench, taxiing experiments are conducted to verify the theoretical results regarding the influence of strut height variation on landing gear stability. The research shows that the theoretical model presented in this paper is reliable. The stable region of landing gear shimmy increases as the strut height decreases. When the landing gear is in a stable convergent state, under a certain external excitation, reducing the strut height can increase the convergence speed of the landing gear and reduce the total vibration amplitude. Combined with experimental conclusions, the theoretical results are verified, clarifying that reducing strut height is one of the ways to improve the taxiing stability of the nose landing gear, providing experimental basis and guidance for the structural optimization and performance improvement of subsequent unmanned aircraft nose landing gears.

Keywords

Landing Gear, Shimmy, Stability, Shimmy Experiment, Simulation Analysis, Strut Height

1. Introduction

Aircraft landing gear is a critical system that directly affects flight safety and

ground operational performance. During taxiing, takeoff, and landing, the landing gear is subjected to complex dynamic loads. Among these, shimmy—a self-excited oscillation—is a typical instability phenomenon in the landing gear system. Shimmy is characterized by coupled torsional and lateral vibrations of the strut and wheels, primarily induced by the interaction between the elastic tires and the runway surface [1]. Therefore, effectively suppressing shimmy and enhancing the dynamic stability of the landing gear have become key issues in landing gear design and airworthiness certification.

Over the years, extensive research has been conducted on landing gear shimmy dynamics, resulting in the development of various dynamic models. Early work by Von Schlippe and Dietrich [2] introduced the stretched string tire model, which remains a foundational theory for tire dynamics in shimmy analysis. Moreland [3] and Smiley [4] further contributed to tire modeling with the point contact theory and comprehensive linearized analyses. Building on these tire models, researchers have progressively developed multi-degree-of-freedom shimmy dynamic models. Thota *et al.* [5] established a three-degree-of-freedom nonlinear model incorporating torsional, lateral, and longitudinal strut motions and analyzed various types of shimmy oscillations using bifurcation theory.

The nonlinear characteristics of landing gear systems have also received increasing attention. Coulomb friction, freeplay, and shock absorber nonlinearities are key factors influencing shimmy stability. Rahmani and Behdinan [6] investigated the interaction between torque link freeplay and Coulomb friction nonlinearities, demonstrating that the presence of freeplay leads to the emergence of a new region characterized by low-amplitude rotational oscillations and zero steady-state lateral amplitude.

Structural parameters such as strut height also play a crucial role in landing gear shimmy stability. Xiao *et al.* [7] developed a nonlinear dynamic model considering strut height and validated the relationship between strut slenderness ratio and critical shimmy speed through experiments. Sivakumar *et al.* [8] established a coupled dynamic model integrating tricycle landing gear with aircraft structure, revealing the coupling effects between airframe motions and landing gear modes. Ruan *et al.* [9] investigated the influence of tire contact deformation and pavement curvature on shimmy stability, demonstrating that tire imprint parameters significantly affect the critical damping required for shimmy suppression.

In view of the above, this paper takes a certain aircraft nose landing gear as the research object and establishes a four-degree-of-freedom dual-wheel nose landing gear shimmy dynamic model considering strut height variation. The relationship between strut stiffness and strut height is verified through static simulation analysis. Using bifurcation analysis methods, the influence of strut height variation on the stable region and stability performance of the landing gear is analyzed. Frequency spectra are used to analyze the dominant frequency of landing gear shimmy and the effect of strut height on vibration energy. Finally, taxiing experiments are conducted on a simulation test bench to verify the theoretical results.

This study provides experimental basis and guidance for the structural optimization and performance improvement of nose landing gears.

2. Modeling of the Landing Gear Shimmy Model

2.1. Dynamic Model of Landing Gear Shimmy

In this paper, the influence of strut height on landing gear stability is analyzed for a certain aircraft nose landing gear. The structural diagram of the landing gear system is shown in Figure 1. This section establishes a four-degree-of-freedom landing gear model, where the degrees of freedom are: strut torsional angle θ, lateral bending angle ϕ, and lateral displacements of the two wheels Δ_L and Δ_R. First, a global coordinate system $OXYZ$ is established with the fixed point o of the landing gear as the origin. The positive X-axis is in the direction of taxiing, the Y-axis is lateral, and the Z-axis is perpendicular to the ground. In Figure 1(a), point o represents the connection point between the landing gear and the fuselage, a is the distance between the center points of the left and right tires, H is the distance from the fixed point to the tire-ground contact point, *i.e.*, the landing gear height, and L_1 is the length of the strut outer cylinder. In Figure 1(b), δ is the angle between the strut axis and the global Z-axis, R is the wheel radius, e is the mechanical caster length (distance from the wheel center to the strut axis), and e_{eff} is the effective caster length. In Figure 1(c), φ is the angle between the wheel yaw direction and the taxiing direction (X-axis), M_t is the moment acting on the strut generated by the tire-ground interaction, F_n is the lateral force generated by tire lateral displacement and wheel deformation, k_θ is the strut torsional stiffness coefficient, c_θ is the strut torsional damping coefficient, and c_{sh} is the damping coefficient provided by the shimmy damper. In Figure 1(d), V is the taxiing speed, η is the tire slip angle, σ is the tire relaxation length, and a_1 is the half-length of the tire contact patch, where the yaw angle can be expressed as $\varphi = \theta\cos(\delta)$. The values of the parameters are shown in Table 1.

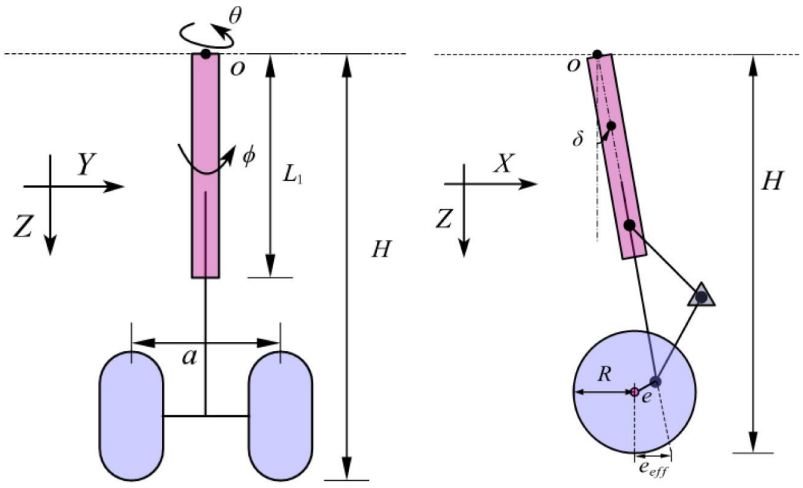

(a) (b)

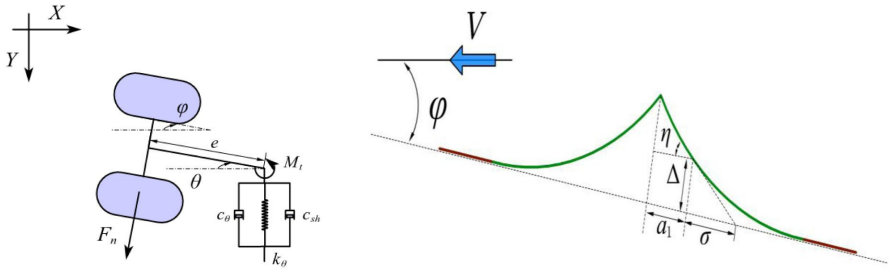

(c) (d)

Figure 1. Landing gear structural diagram. (a) Front view; (b) Side view; (c) Top view.

Before establishing the shimmy model, the assumptions and definitions presented in this paper are as follows:

(1) The landing gear wheels do not separate from or slip on the ground.

(2) The influence of the fuselage on landing gear shimmy is neglected, and it is equivalent to a constant vertical load.

(3) Only the effect of strut height variation on the strut stiffness coefficient is considered, while the effects of its geometry, inertia, and other factors are neglected.

Thus, a nonlinear four-degree-of-freedom dual-wheel landing gear shimmy dynamic model is established, describing the strut torsion, lateral bending, and the equations for the left and right wheels as follows:

$$\begin{aligned} &I_\theta\ddot{\theta}+C_\theta\dot{\theta}+K_\theta\theta+M_{k_{\eta L}}+M_{k_{\eta R}}-F_{zL}\sin(\delta)\left(L_{eff}\sin(\varphi)+\frac{D}{2}\cos(\varphi)+H\sin(\phi)\right)\\ &-F_{zR}\sin(\delta)\left(L_{eff}\sin(\varphi)-\frac{D}{2}\cos(\varphi)-H\sin(\phi)\right)+M_{D_{\Delta\theta L}}+M_{D_{\Delta\theta R}}+2I\frac{V}{R}\dot{\phi} \end{aligned} \tag{1}$$

$$\begin{aligned} &I_\phi\ddot{\phi}+C_\phi\dot{\phi}+K_\phi\phi+M_{\Delta_{\phi L}}+M_{\Delta_{\phi R}}+M_{D_{\Delta\phi L}}+M_{D_{\Delta\phi R}}\\ &-F_{zL}\left(L_{eff}\sin(\varphi)+\frac{D}{2}\cos(\varphi)+H\sin(\phi)\right)\\ &-F_{zR}\left(L_{eff}\sin(\varphi)-\frac{D}{2}\cos(\varphi)-H\sin(\phi)\right)-2I\frac{V}{R}\dot{\theta} \end{aligned} \tag{2}$$

$$\begin{aligned} &\dot{\Delta}_L+\frac{V}{\sigma}\Delta_L-V\sin(\varphi)-H\cos(\phi)\dot{\phi}\\ &-\left(L_{eff}-h\right)\cos(\varphi)\cos(\delta)\dot{\theta}-\frac{D}{2}\sin(\varphi)\cos(\delta)\dot{\theta}=0 \end{aligned} \tag{3}$$

$$\begin{aligned} &\dot{\Delta}_R+\frac{V}{\sigma}\Delta_R-V\sin(\varphi)-H\cos(\phi)\dot{\phi}\\ &-\left(L_{eff}-h\right)\cos(\varphi)\cos(\delta)\dot{\theta}+\frac{D}{2}\sin(\varphi)\cos(\delta)\dot{\theta}=0 \end{aligned} \tag{4}$$

The influence of the strut lateral bending angle on tire lateral deformation can be expressed as: $\theta=\psi\cos(\phi+\beta)$. Here, ψ and β represent the strut torsional angle and the sideslip angle generated by the landing gear rotating around the fuselage, respectively. M_{nL} and M_{nR} are the nonlinear self-aligning moments of the left and right tires, k_α is the tire nonlinear self-aligning moment

coefficient, and α_m is the limit slip angle of the wheel. F_{zL} and F_{zR} are the vertical forces acting on the left and right tires, respectively. The landing gear tilt angle can be expressed as $\beta = \theta \sin(\delta)$.

$$M_{k_{\eta L}} = \begin{cases} C_{M_\eta L/R} F_{Zi} \left(\frac{\eta_m}{180^\circ}\right) \sin\left(\frac{180^\circ}{\eta_m} \eta_{L/R}\right) & |\eta_{L/R}| \le \eta_m \\ 0 & |\eta_{L/R}| \ge \eta_m \end{cases} \tag{5}$$

$$\begin{aligned} F_{zL} &= \frac{F_z}{2}\left[1 \mp \left(\frac{k_v(p_{L/R})D}{F_z}\right)\sin(\gamma+\phi)\right] \\ &= \frac{F_z}{2}\left[1 \mp \left(\frac{k_v(p_{L/R})D}{F_z}\right)\sin(\theta\sin(\delta)+\phi)\right] \end{aligned} \tag{6}$$

According to the tire lateral stiffness coefficient, vertical force, and tire slip angle, the tire lateral restoring force $F_{nL/R}$ can be obtained. The tire slip angle $\eta_{L/R}$ is given by the following formula:

$$F_{n_{L/R}} = k_\lambda \tan^{-1}\left(7.0\tan\left(\eta_{L/R}\right)\right)\cos\left(0.95\tan^{-1}\left(7.0\tan\left(\eta_{L/R}\right)\right)\right)F_{zL/R} \tag{7}$$

$$\eta_{L/R} = \arctan\left(\frac{\Delta_{L/R}}{\sigma}\right) \approx \frac{\Delta_{L/R}}{\sigma} \tag{8}$$

The effective caster length e_{eff} of the landing gear is given by:

$$e_{eff} = e\cos(\delta) + \left(R + e\sin(\delta)\right)\tan(\delta) \tag{9}$$

$M_{D\Delta\theta L/R}$ is the damping moment between the tire tread and the ground, whose magnitude is determined by the taxiing speed, the tire damping coefficient, and the wheel yaw angle. $M_{D\Delta\theta L/R} = c_\lambda \dot{\theta}/V$. $M_{\Delta\phi L}$ and $M_{\Delta\phi R}$ are the strut lateral moments generated by the tire-ground interaction.

$$M_{\Delta\phi L/R} = HF_{n_{L/R}}\cos(\varphi)\cos(\delta) \tag{10}$$

2.2. Tire Model

This section lists a series of relationships between normalized tire inflation pressure and tire vertical stiffness, tire self-aligning moment coefficient, tire torsional damping coefficient, tire lateral damping coefficient, etc. The normalized tire inflation pressure is defined as $p_{L/R} = p_{1L/R}/p_e$, where $p_{1L/R}$ is the current inflation pressure of the left and right tires, and p_e is the rated tire inflation pressure. When $p_{L/R} = 1$, the current tire pressure is equal to the rated pressure.

(1) Relationship between tire contact patch length and tire inflation pressure: The tire contact patch length mainly affects the torsional and lateral damping moments of the left and right tires.

$$h_{L/R} = R\sqrt{1 - \left(1 - \frac{F_{zL/R}}{k_{v_{L/R}} R}\right)^2} \tag{11}$$

(2) Relationship between tire relaxation length and tire inflation pressure: The

relationship between tire relaxation length and tire inflation pressure is shown in Eq. (12).

$$\sigma_{L/R} = \left(2.8 - 0.8 p_{L/R}\right)\left(1 - 2.25\frac{F_{zL/R}}{k_{vL/R}R}\right)w \tag{12}$$

(3) Relationship between tire self-aligning moment coefficient and tire inflation pressure: During taxiing, the wheel interacts with the ground, causing tire deformation and generating a self-aligning moment, where $C_{M\eta}$ is the tire nonlinear self-aligning moment coefficient, mainly acting on the nonlinear tire self-aligning moment.

$$C_{M_\eta} = 2.0539 - 1.0823 p_{L/R} \tag{13}$$

Relationship between tire vertical stiffness and tire inflation pressure: Each type of wheel has a default vertical stiffness k_v, and the tire vertical stiffness $k_{vL/R}$ increases linearly with tire inflation pressure.

$$k_{v_{L/R}} = \left(0.813 p_{L/R} - 0.024\right)k_v \tag{14}$$

Relationship between tire damping force and tire inflation pressure: $C_{tL/R}$ is the tire torsional damping coefficient, which is linearly related to tire pressure.

$$C_{tL/R} = 0.1432 p_{L/R} + 0.1067 \tag{15}$$

The expression for the tire torsional damping moment is shown in Eq. (16):

$$M_{D_{\Delta\theta L/R}} = \frac{C_{tL/R}C_{M_\eta}\left(h_{L/R}/2\right)^2 F_{zL/R}}{V}\dot{\theta} \tag{16}$$

The relationship between the tire lateral damping coefficient and tire inflation pressure is as follows: as the tire inflation pressure increases, the tire lateral damping coefficient decreases linearly.

$$C_{lL/R} = -0.1909 p_{L/R} + 0.3609 \tag{17}$$

The expression for the tire lateral damping moment is shown in Eq. (18):

$$M_{D_{\Delta\phi L/R}} = \frac{C_{lL/R}k_\lambda h_{L/R}^2 F_{zL/R}}{V}\dot{\phi} = \left(-0.1909 p_{L/R} + 0.3609\right)\frac{k_\lambda h_{L/R}^2 F_{zL/R}}{V}\dot{\phi} \tag{18}$$

Table 1. Parameters of the nonlinear landing gear shimmy model.

Parameters	Definitions	Values	Units
e	Caster length	0.12	m
I_θ	Strut torsional moment of inertia	100	Kg·m^2
I_ϕ	Strut lateral bending moment of inertia	600	Kg·m^2
I	Wheel moment of inertia	0.8	Kg·m^2
K_θ	Strut torsional moment of inertia	-	N·m/rad
K_ϕ	Strut lateral bending stiffness	-	N·m/rad
C_θ	Strut torsional damping	20	N·m·s/rad

Continued

C_ϕ	Strut lateral bending damping	300	N·m·s/rad
C_{sh}	Shimmy damper damping	280	N·m·s/rad
δ	Rake angle	0.1571	rad
H	Landing gear height	0.5	m
w	Tire width	0.245	m
R	Wheel radius	0.362	m
D	Distance between wheel center points	0.3	m
p	Ratio of tire pressure to rated pressure	1	-
k_v	Tire vertical stiffness	4,000,000	N/m
η_m	Maximum slip angle	0.1745	rad
F_z	Vertical load	160,000	N
V	Velocity	0 - 200	m/s

2.3. Relationship between Strut Height and Stiffness

Based on the mechanics of materials, this section establishes the relationship between landing gear strut stiffness and strut height. The variation in strut height is achieved by changing the length of the strut outer cylinder; therefore, only the change in the length of the strut outer cylinder is discussed hereafter. Here, the landing gear height includes the tire height, the strut height is the distance from the wheel axle to the landing gear attachment point excluding the tire, and the strut outer cylinder length refers to the part of the landing gear equipped with the shock absorber. Meanwhile, the values of some parameters are shown in Table 2.

(1) **Lateral bending stiffness coefficient of strut** k_δ**:** According to data from a certain aircraft landing gear, the outer diameter of the strut outer cylinder is $d_1 = 0.2$ m, the inner diameter is $d_2 = 0.17$ m, the length of the strut outer cylinder is $L_1 = 1.688$ m, the diameter of the strut inner cylinder is $d_3 = 0.09$ m, and its length is $L_2 = 0.629$ m. Since the landing gear material is 300 M steel, the elastic modulus is $E = 210$ GPa. The lateral bending stiffness of the strut K_1 is 3.1225×10^6 N/m, and the expression is given by Eq. (19):

$$K_\phi = 1 \Bigg/ \left(\frac{(L_1)^3}{3E\dfrac{\pi(d_1 - d_2)^4}{64}} + \frac{(L_2)^3}{3E\dfrac{\pi d_3^4}{64}} \right) \tag{19}$$

(2) **Torsional stiffness coefficient of strut** k_ψ**:** The strut is modeled as a circular rod parallel to its axis, where relative rotation can occur between the inner and outer cylinders. Here, the torsional stiffness of the strut outer cylinder and the wheel rod is considered. According to the landing gear data, the outer diameter of the strut outer cylinder is $d_o = 0.2$ m, inner diameter $d_i = 0.17$ m, length of the strut outer cylinder $L_o = 1.688$ m, the equivalent diameter of the wheel rod is $d_r = 0.07$ m, and its length is $L_r = 0.3757$ m. The shear modulus

$G = 80$ GPa is substituted into Eq. (20), giving a result of 4.3988×10^5 N·m/rad. Thus, the expression for the torsional stiffness coefficient is:

$$K_\theta = 1 \Bigg/ \left(\frac{L_1}{G\frac{\pi(d_1 - d_2)^4}{32}} + \frac{L_3}{G\frac{\pi d_4^4}{32}} \right) \tag{20}$$

Table 2. Parameters related to the landing gear strut structure.

Parameters	Definitions	Values	Units
d_1	Outer diameter of strut outer cylinder	0.2	m
d_2	Inner diameter of strut outer cylinder	0.17	m
d_3	Diameter of strut inner cylinder	0.09	m
d_4	Diameter of wheel rod	0.07	m
E	Elastic modulus	210	Mpa
G	Shear modulus	8	Mpa
L_1	Length of strut outer cylinder	1.688	m
L_2	Length of strut inner cylinder	0.619	m
L_3	Equivalent length of wheel rod	0.3757	m
I_1	Moment of inertia of strut outer cylinder	-	Kg·m^2
I_2	Moment of inertia of strut inner cylinder	-	Kg·m^2
J_1	Distance between wheel center points	-	Kg·m^2
J_2	Ratio of tire pressure to rated pressure	-	Kg·m^2

To verify the theoretical model proposed in this paper, the theoretical results are compared with the simulation analysis results, analyzing the agreement and error between them. The strut structure of a certain aircraft nose landing gear is shown in **Figure 2**, including an assembly diagram of the fixture and the landing gear strut, which allows adjustment of the strut length. Since domestic and foreign aircraft landing gear often use 300 M (40CrNi2Si2MoVA) steel as the main material, the landing gear model provided in this paper also uses 300 M steel as the structural material.

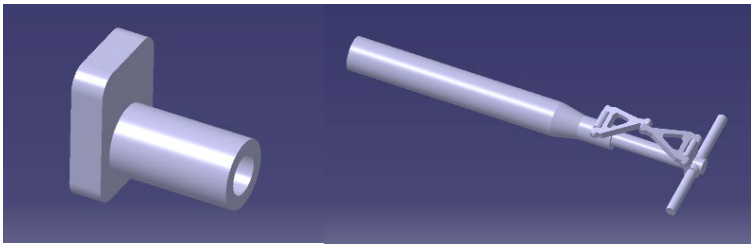

(a) (b)

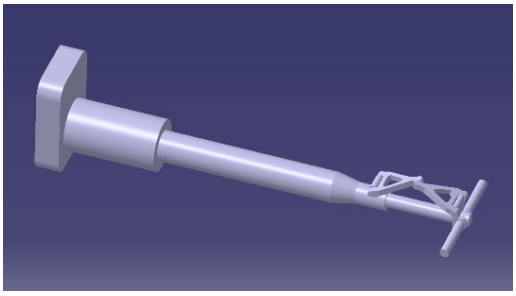

(c)

Figure 2. Numerical models of the landing gear strut and fixture. (a) Assembled landing gear with fixture; (b) Landing gear fixing fixture; (c) Assembled overall landing gear model.

The numerical model was imported into Ansys. After verification, it was found that the landing gear structure has a stress margin area, and the landing gear strength is appropriate. Then, a lateral displacement of 0.01 m was applied at the wheel rod to obtain the strut lateral bending stiffness through linear static analysis. Similarly, a moment of 10,000 N·m was applied at both ends of the landing gear wheel rod to obtain the strut torsional stiffness. By adjusting the strut length (six different working conditions for each type of stiffness measurement), the simulation results were compared with the theoretical model results, and the errors were analyzed. The results are given in **Table 3** and **Table 4**.

Table 3. Comparison of simulation and theoretical values of lateral bending stiffness coefficient.

Reduction in strut height (m)	Theoretical lateral bending stiffness (N/m)	Simulation result (N/m)	Error (%)
0	3,122,200	3,122,250	0
0.1	3,493,500	3,540,900	1.3
0.2	3,902,800	4,026,100	3.0
0.3	4,348,000	4,601,500	5.6
0.4	4,824,600	5,266,200	8.3
0.5	5,324,300	6,036,100	11.7

Table 4. Comparison of theoretical and simulated values of torsional stiffness.

Reduction in strut height (m)	Theoretical lateral bending stiffness (N/m)	Simulation result (N/m)	Error (%)
0	439,890	439,899	0
0.1	443,130	442,504	0.1
0.2	446,420	444,912	0.3
0.3	449,770	447,553	0.5
0.4	453,160	450,226	0.7
0.5	456,610	452,931	0.8

From the results in the table, it can be seen that the error in the lateral bending stiffness of the strut increases with increasing strut height. The main reason for this error is that the theoretical model does not consider the lateral stiffness contributed by the wheel axle and the torque links. The error in the torsional stiffness of the strut also increases with increasing strut height. Here, the torque links are considered as rigid bodies that only transmit torque, which leads to the error. In summary, the smaller the change in strut height, the smaller the error between the theoretical and simulation results, and the more reliable the theoretical model.

3. Influence of Strut Height on Landing Gear Stability

In this section, the numerical analysis of the landing gear shimmy model is carried out using the MTCONT tool, with the initial conditions of all state variables set to zero. Based on the landing gear shimmy model established above, the taxiing speed of the aircraft and the equivalent vertical load of the fuselage are selected as continuation parameters to plot two-parameter bifurcation diagrams. The variation in strut height is achieved by changing the length of the strut outer cylinder, thereby analyzing the influence of strut height on landing gear stability. Furthermore, the strut outer cylinder height and the taxiing speed are selected as continuation parameters for a two-parameter bifurcation analysis to examine the stable region. To determine whether landing gear shimmy occurs, it can be assessed by checking whether the dynamic model of landing gear shimmy undergoes a Hopf bifurcation. Frequency spectra are used to analyze the influence of strut height variation on vibration frequency and amplitude.

3.1. Bifurcation Analysis

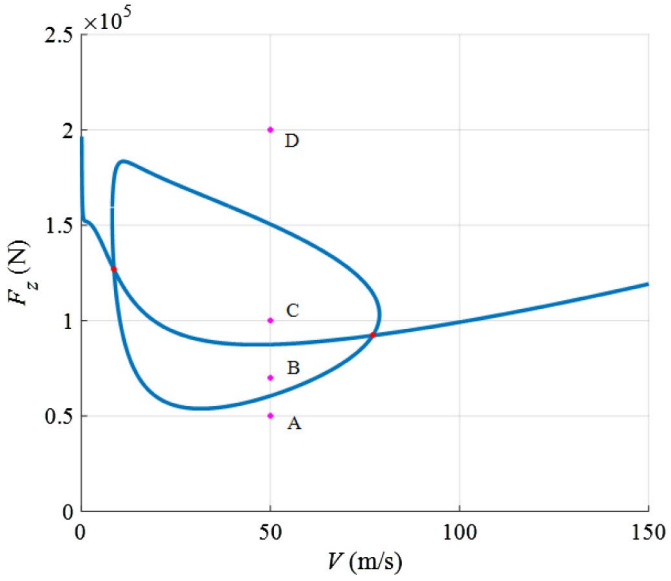

Figure 3. Two-parameter bifurcation diagram of landing gear shimmy in the (V, F_z) plane.

Based on the four-degree-of-freedom landing gear shimmy dynamic model, the parameter data shown in Table 1 and Table 2 are used as the input data for plotting the bifurcation diagrams. The taxiing speed and the vertical load are selected as continuation parameters to plot the two-parameter bifurcation diagram in Figure 3. The diagram consists of two blue curves, with the red points indicating the intersections of the two curves, *i.e.*, the double Hopf points. The fully closed curve represents the torsional shimmy curve, while the other curve represents the lateral shimmy curve. To verify the stability of each region, the diagram is divided into four regions (1, 2, 3, and 4), and four points (A - D) are selected, as shown in Figure 3. Finally, the stability of the regions is validated through time history diagrams and phase portraits.

Among them, the taxiing speed for points A to D is 50 m/s, and the vertical loads are 50 kN, 70 kN, 100 kN, and 200 kN, respectively, while other parameters remain unchanged. Based on this, the phase portraits and time histories are calculated, as shown in Figure 4.

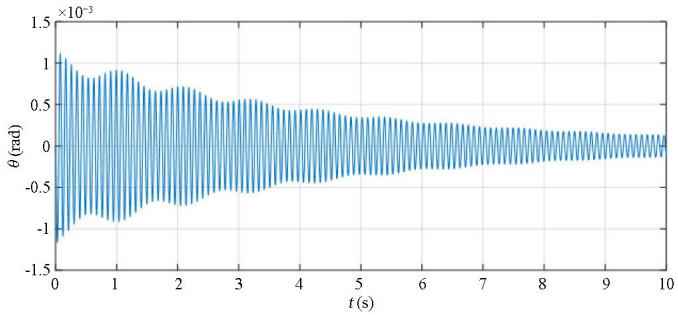

(a)

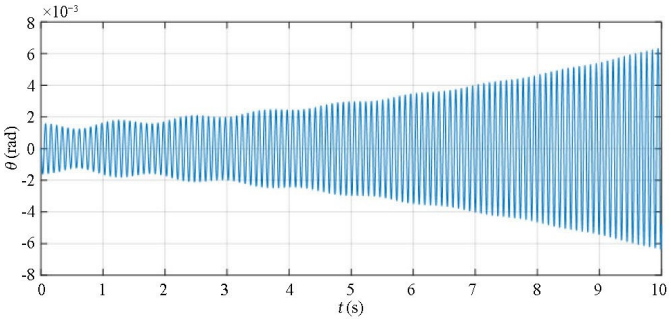

(b)

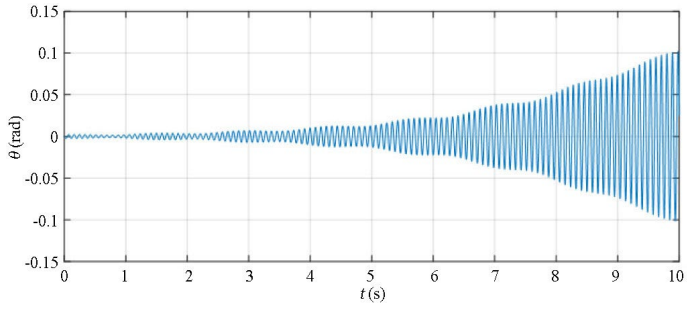

(c)

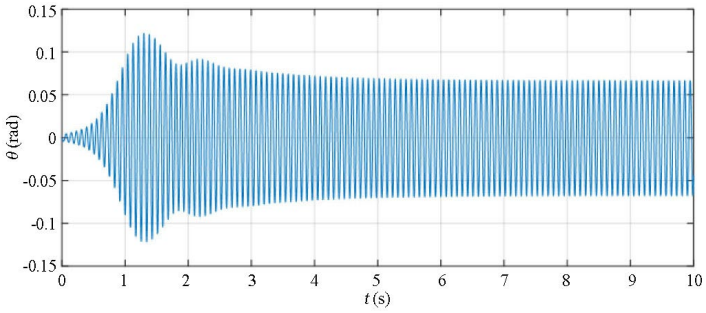

(d)

Figure 4. Time history and phase diagrams of the selected points in different regions of the bifurcation diagram (a) Time history at point A (b) Time history at point B (c) Time history at point C (d) Time history at point D.

Figure 4 shows the time histories of the strut torsion. From the time history diagrams, it can be seen that the amplitude in the region of point A is stable and convergent, while the strut torsion angle in the regions of the other points increases continuously. It can be concluded that the region containing point A is a stable region, whereas the other regions are unstable.

In this section, two-parameter bifurcation diagrams with speed and vertical load as continuation parameters, as well as time history curves, are plotted to analyze the influence of reducing the length of the strut outer cylinder on landing gear stability. **Figure 3(a)** is the two-parameter bifurcation diagram for torsional shimmy, and **Figure 3(b)** is for lateral shimmy.

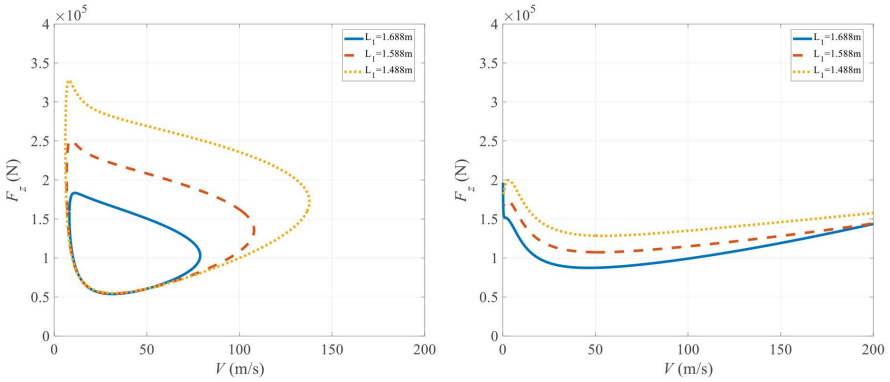

(a) (b)

Figure 5. Two-parameter bifurcation diagrams in the (V, F_z) plane. (a) Torsional shimmy two-parameter bifurcation diagram; (b) Lateral shimmy two-parameter bifurcation diagram.

From the results in **Figure 5**, it can be seen that the stable region of landing gear shimmy increases as the length of the strut outer cylinder decreases (*i.e.*, as the strut height decreases). Therefore, without considering the influence of landing gear height on the overall center of gravity of the aircraft, reducing the strut height can significantly improve the shimmy stability of the landing gear.

Selecting the taxiing speed V and the strut outer cylinder length L_1 as continuation parameters, the two-parameter bifurcation diagram in the (V, L_1) plane is plotted in Figure 6. This diagram consists of a blue curve and a purple curve, each drawn from a Hopf point. The purple curve is drawn from the first Hopf point, and the blue curve is drawn from the second Hopf point.

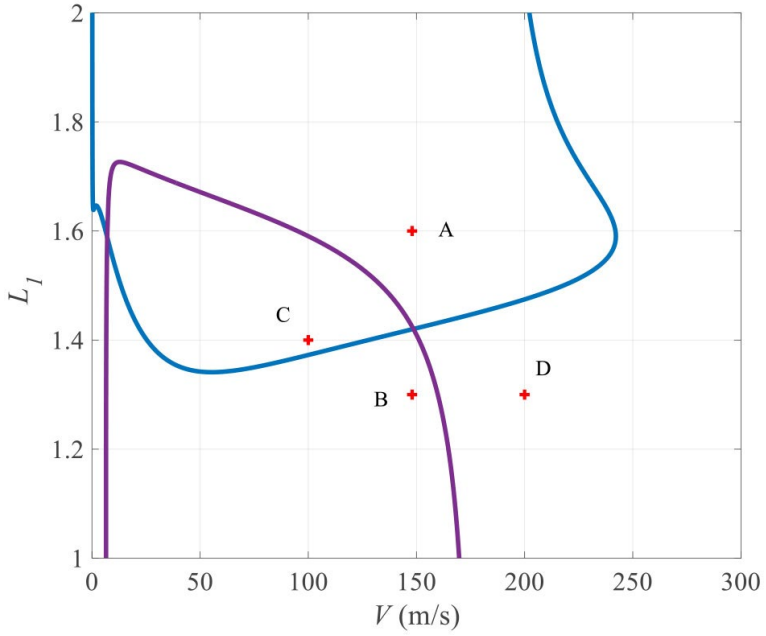

Figure 6. Two-parameter bifurcation diagram of landing gear shimmy in the (V, L_1) plane.

To verify the stability of the regions formed by the intersection of the two curves, four points (A - D) were selected: A [148, 1.6], B [148, 1.3], C [100, 1.4], D [200, 1.3]. The regions where these points are located are divided into Regions 1, 2, 3, and 4. Time history diagrams are plotted according to the given data, as shown in Figure 7. Among them, the initial values of the strut torsion and strut lateral bending in the time history diagrams are zero, and the initial lateral displacements of the left and right tires are both 0.01 m.

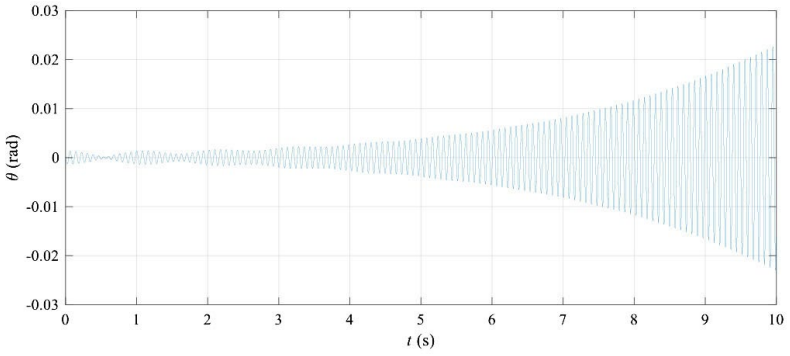

(a)

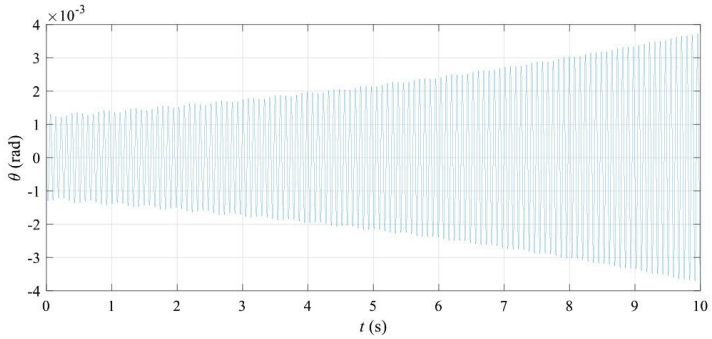

(b)

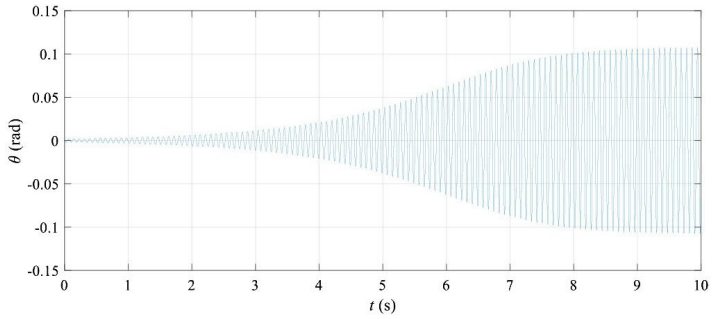

(c)

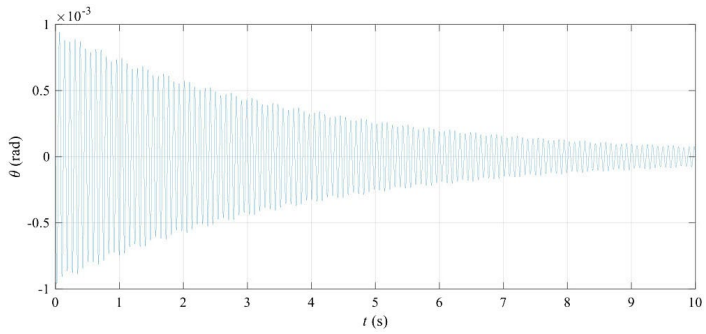

(d)

Figure 7. Time history diagrams. (a) Time history at point A; (b) Time history at point B; (c) Time history at point C; (d) Time history at point D.

From Figure 7, it can be seen that at point A, the torsional amplitude of the strut initially fluctuates but eventually diverges significantly; at point B, the amplitude continuously diverges; at point C, the amplitude diverges rapidly; at point D, the torsional amplitude of the strut clearly converges, and the overall amplitude continuously decreases. This indicates that among the four regions, only Region 4 is a stable region.

3.2. Time Domain Analysis

In this subsection, a set of stable points from Figure 5 is selected. Except for the variation of strut height, the other values remain consistent with those in the table. Here, the taxiing speed is 50 m/s, and the vertical load is 50 kN. Thus, as the strut height decreases, the time history diagrams corresponding to different landing

gear heights are plotted, as shown in Figure 8. In these diagrams, the initial values of strut torsion and strut lateral bending are zero, and the initial lateral displacements of the left and right tires are both 0.01 m.

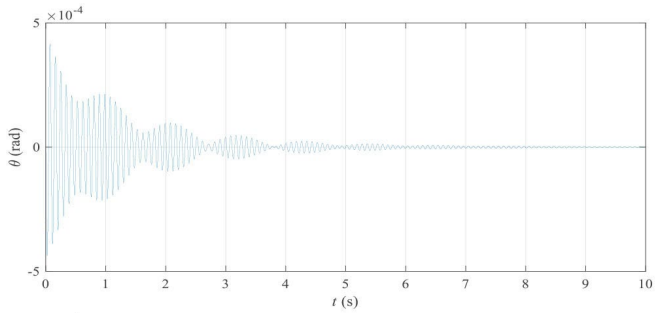

(a)

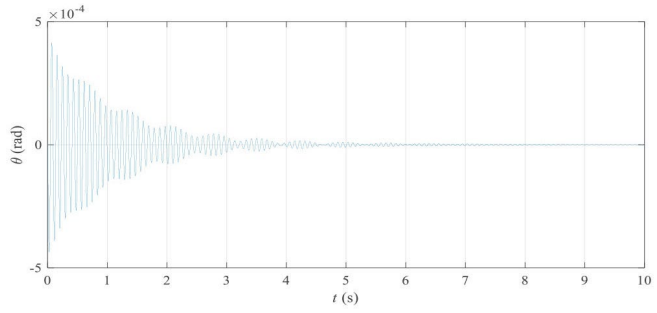

(b)

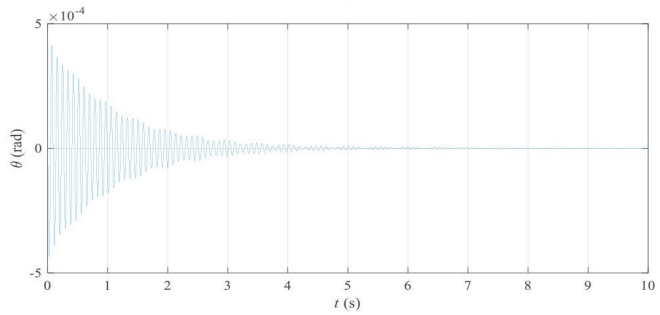

(c)

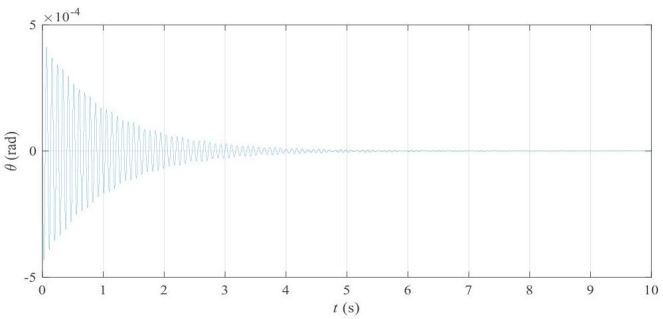

(d)

Figure 8. Time history and phase plane diagra ms for points in each region. (a) Time history for $L_1 = 1.688$ m; (b) Time history for $L_1 = 1.588$ m; (c) Time history for $L_1 = 1.488$ m; (d) Time history for $L_1 = 1.388$ m.

It can be seen from Figure 8 that as the length of the strut outer cylinder decreases, the amplitude of the time history diagram does not change significantly, but the fluctuation of the amplitude is greatly suppressed. After 10 seconds, the amplitudes converge to 0 rad. Moreover, as the strut height decreases, the convergence time of the time history diagram becomes shorter, *i.e.*, the convergence speed increases. This indicates that reducing the strut height makes the landing gear converge more stably.

3.3. Steady-State Frequency Analysis

Here, points in Region 4 are selected, where the landing gear is stable during taxiing. The frequency spectra are used to compare the vibration states of the landing gear at different strut heights, as listed in Table 5.

Table 5. Numerical values correspond to the selected parameter points.

Parameter Point No.	V (m/s)	L_1 (m)
A1	200	1.42
A2	200	1.32
A3	200	1.22

By performing fast Fourier transform on the time history data, the frequency spectra for each degree of freedom corresponding to each parameter point are obtained, as shown in the figures below. These include the spectra for torsion, lateral bending, and lateral deformation of the left and right wheels. Selecting data points in the stable region, the relationship between the landing gear damping natural frequency and the strut outer cylinder length is observed by varying the strut length, as shown in Figure 7.

It can be seen from Figure 9(a)-(d) that the frequency spectra of the four degrees of freedom corresponding to the three points all have two peaks. As the length of the strut outer cylinder decreases, the peak frequencies in the spectra increase. By analyzing the first three peaks and the last three peaks in each graph, it can be observed that when the length of the strut outer cylinder decreases, the amplitudes of the first three peaks increase slightly, while the amplitudes of the last three peaks decrease significantly, and the overall amplitude is always decreasing, *i.e.*, the vibration energy decreases. Meanwhile, except for the lateral shimmy frequency, the other dominant frequencies first decrease and then increase slightly as the strut height decreases, whereas the dominant frequency of lateral shimmy always increases. This indicates that when the landing gear is stable without shimmy and a certain initial condition is provided, the sum of the vibration amplitudes of each degree of freedom of the landing gear in the frequency domain decreases as the strut outer cylinder length decreases, *i.e.*, the total vibration energy decreases significantly.

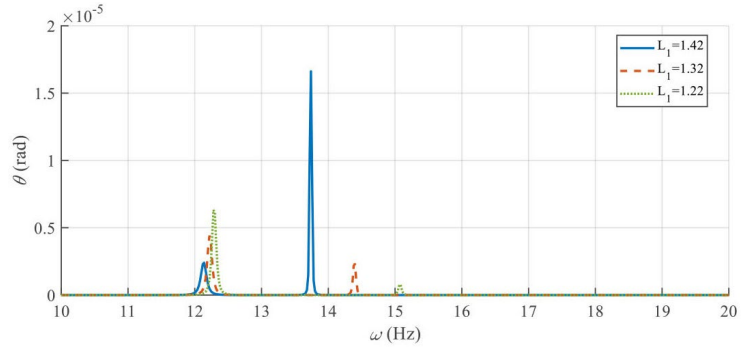

(a)

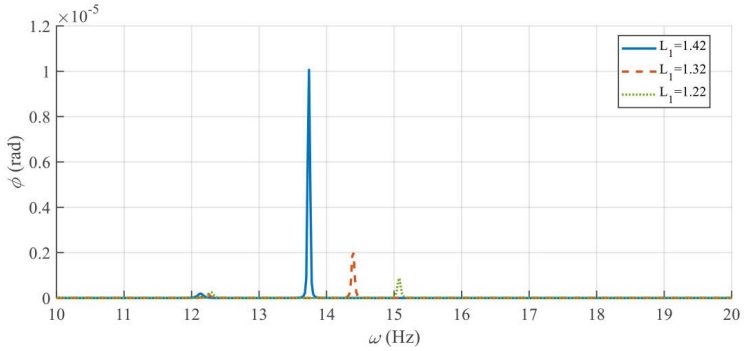

(b)

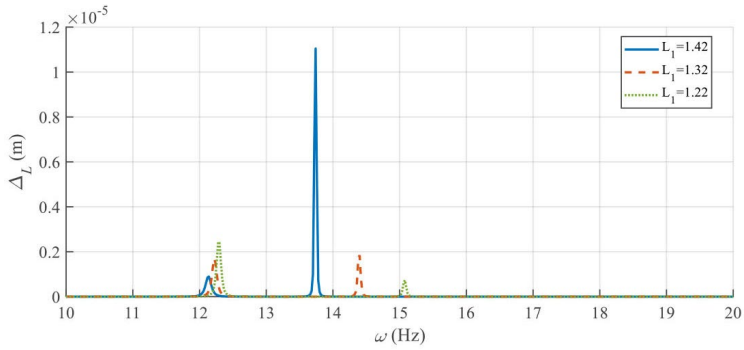

(c)

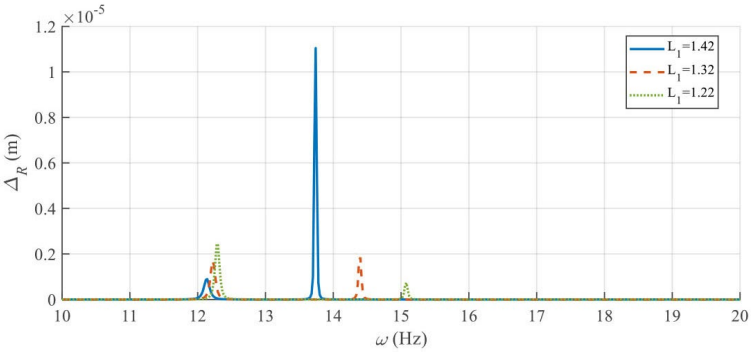

(d)

Figure 9. Frequency spectra of the four degrees of freedom for points in different shimmy regions. (a) Torsional deformation spectrum; (b) Lateral bending deformation spectrum; (c) Left wheel lateral deformation spectrum; (d) Right wheel lateral deformation spectrum.

4. Taxiing Simulation Experiment

4.1. Experimental Setup

The shimmy test bench used in this chapter is an indoor flywheel-type shimmy test bench, as shown in Figure 10. The shimmy test bench includes a flywheel, a servo motor, and a lifting mechanism. Data measurement and processing are performed using a laser vibrometer. The performance parameters of each device are listed in Table 6.

Table 6. Parameters of the shimmy test bench and required equipment.

No.	Equipment Name	Main Performance Indicators
1	Flywheel	Rated speed: 144 km/h
2	Servo motor	Power; voltage 220 V
3	Lifting mechanism	Stroke 1500 mm
4	Laser vibrometer (PSV-500-1D)	Maximum sampling frequency: 25 kHz

(a) (b)

Figure 10. Landing gear test bench and measurement instruments. (a) Landing gear installed; (b) Landing gear test in progress.

The taxiing simulation experiment procedure for the landing gear is as follows: First, install the landing gear and adjust the lifting mechanism to apply the same vertical displacement to the landing gear, which can be determined by measuring the extension and retraction of the landing gear support strut. Second, in the control center of the laser vibrometer, adjust the laser vibrometer properly, complete the instrument inspection, and select the lateral strut surface of the landing gear as the measurement area. Finally, start the motor via the motor control panel to reach the target speed, activate the laser vibrometer, and complete the taxiing simulation test and data processing after approximately 3 minutes.

4.2. Experimental Results

A shimmy experiment on a certain unmanned aircraft nose landing gear with var-

iable stiffness was conducted. By changing the relative displacement between the strut and the fixture, variable stiffness was achieved to verify the influence of strut height variation on landing gear stability.

(a) (b) (c)

Figure 11. Different settings of strut outer cylinder height. (a) H1; (b) H2; (c) H3.

The landing gear stiffness was achieved by adjusting the relative distance between the strut outer cylinder length and the fixture, and fixing it with screws, as shown in Figure 11. The initial strut outer cylinder length was 20 cm, changed twice, each change being 3 cm. There were three groups of different working conditions: H1, H2, and H3, totaling 12 different conditions. H1, H2, and H3 correspond to strut outer cylinder lengths of 17 cm, 14 cm, and 11 cm, respectively. The specific working conditions are shown in Table 7.

Table 7. Shimmy experiment scheme with varying strut outer cylinder length.

Parameters	Definitions	Flywheel speed (m/s)
1	H1 = 17	5
2		10
3		15
4		20
5	H2 = 14	5
6		10
7		15
8		20
9	H3 = 11	5
10		10
11		15
12		20

According to the 12 working conditions listed above, following the test procedures and specifications, the shimmy experiments were completed. From the experimental results, the relationship curves between the flywheel speed V and the dominant frequency f of the nose landing gear system, as well as the amplitude A corresponding to the dominant frequency, were plotted, as shown in Figure 12.

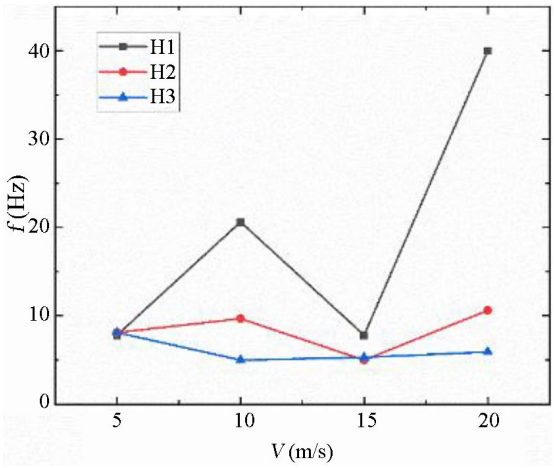

(a)

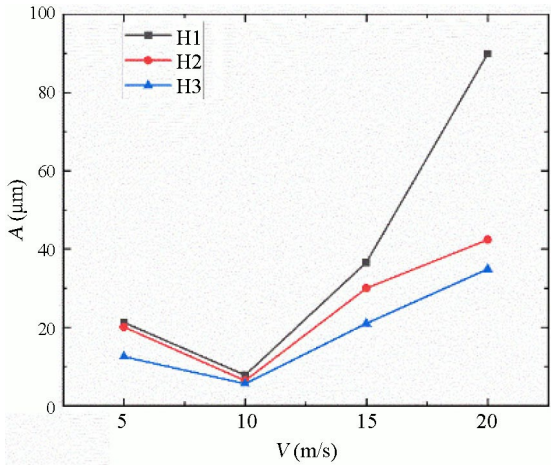

(b)

Figure 12. Results of nose landing gear shimmy experiments with varying strut outer cylinder length. (a) Comparison of dominant frequency; (b) Comparison of amplitude corresponding to dominant frequency.

As shown in **Figure 12(a)**, when the length of the landing gear strut outer cylinder is H1 or H2, the dominant frequency of the landing gear lateral vibration first increases, then decreases, and finally increases again as the flywheel speed increases from 5 m/s to 20 m/s. When the strut outer cylinder length is H3, the dominant frequency of the landing gear lateral vibration first decreases and then continuously increases as the flywheel speed increases from 5 m/s to 20 m/s. At a given speed, except when the flywheel speed is 5 m/s, as the strut outer cylinder length decreases, the dominant frequency of the landing gear lateral vibration also decreases to a certain extent, fluctuating around 10 Hz. At different flywheel speeds, as the strut outer cylinder length decreases, the vibration amplitude corresponding to the dominant frequency is significantly reduced, and the lateral vibration energy of the landing gear decreases with the reduction in strut outer cylinder length, as shown in **Figure 12(b)**.

In summary, reducing the length of the nose landing gear strut outer cylinder

can significantly reduce the lateral vibration amplitude of the landing gear, *i.e.*, reduce the total vibration energy of the landing gear. Meanwhile, in the flywheel speed range of 5 - 20 m/s, the reduction in strut outer cylinder length generally lowers the dominant vibration frequency of the landing gear. Therefore, in landing gear design, reducing the strut outer cylinder length is very beneficial to the stability of the landing gear system.

5. Taxiing Simulation Experiment

This paper proposed the relationship between strut stiffness and strut height and established a four-degree-of-freedom dual-wheel nose landing gear shimmy dynamic model. The reliability of the relationship between strut stiffness and strut height for a certain aircraft nose landing gear was verified. Using bifurcation analysis methods, the influence of strut height variation on the stable region of the landing gear was analyzed, and the dominant frequency of landing gear shimmy and the effect of strut height on vibration energy were analyzed using frequency spectra. Using a taxiing simulation test bench, taxiing experiments were conducted to verify the influence of strut outer cylinder height variation on landing gear stability, confirming the theoretical results. The main conclusions are as follows:

(1) Under the condition of varying strut height, the theoretical model presented in this paper shows good agreement with the simulation results, and the errors are within an acceptable range. As the strut height continuously decreases, the lateral bending stiffness of the landing gear strut continuously increases; as the strut height continuously decreases, the torsional stiffness coefficient of the landing gear strut also continuously increases.

(2) Without considering the influence of landing gear height on the overall center of gravity of the aircraft, the two-parameter bifurcation diagram shows that reducing the strut height can significantly improve the shimmy stability of the landing gear. The stable region of landing gear shimmy increases steadily as the length of the strut outer cylinder decreases (*i.e.*, as the strut height decreases). According to the time history results, as the strut outer cylinder length decreases, the amplitude of the time history does not change significantly, but the fluctuation of the amplitude is greatly suppressed, and after 10 seconds, the amplitudes converge to 0 rad.

(3) When the landing gear is in a stable convergent state, with a certain initial condition and under a certain external excitation, reducing the strut outer cylinder length increases the convergence time of the landing gear. The sum of the vibration amplitudes of each degree of freedom of the landing gear in the frequency domain decreases as the strut outer cylinder length decreases, *i.e.*, the total vibration energy decreases significantly.

(4) According to the experimental results, reducing the length of the landing gear strut outer cylinder can significantly reduce the lateral vibration amplitude of the landing gear, *i.e.*, reduce the vibration energy of the landing gear, verifying

that reducing the strut height can reduce the vibration amplitude of the landing gear, thereby improving the stability performance of the landing gear. Furthermore, in the flywheel speed range of 5 - 20 m/s, the reduction in strut outer cylinder length generally lowers the dominant vibration frequency of the landing gear. Therefore, in landing gear design, reducing the strut outer cylinder length is very beneficial to the stability of the landing gear system.

In summary, strut height has a significant impact on the stable region of the landing gear, and it must be carefully considered in new aircraft designs. Through taxiing simulation experiments, it has been established that reducing the strut outer cylinder length is one of the ways to improve the taxiing stability of the nose landing gear of this unmanned aircraft, providing experimental basis and guidance for the structural optimization and performance improvement of subsequent unmanned aircraft nose landing gears.

Funding

This work is supported by the National Nature and Science Foundation of China under Grant No. 12072140, Natural Science Foundation of Jiangxi Province of China under Grant No. 20202ACBL201003.

Conflicts of Interest

The authors declare no conflicts of interest regarding the publication of this paper.

References

[1] Besselink, I.J.M. (2000) Shimmy of Aircraft Main Landing Gears. Doctoral Thesis, Delft University of Technology. https://resolver.tudelft.nl/uuid:c9fc838d-57a3-4bd5-b414-7bc675785d99

[2] Von Schlippe, B. and Dietrich, R. (1947) Shimmying of a Pneumatic Wheel. NACA TM 1365.

[3] Moreland, W.J. (1954) The Story of Shimmy. *Journal of the Aeronautical Sciences*, **21**, 793-808. https://doi.org/10.2514/8.3227

[4] Smiley, R.F. (1956) Correlation, Evaluation, and Extension of Linearized Theories for Tire Motion and Wheel Shimmy. National Advisory Committee for Aeronautics.

[5] Thota, P., Krauskopf, B. and Lowenberg, M. (2009) Interaction of Torsion and Lateral Bending in Aircraft Nose Landing Gear Shimmy. *Nonlinear Dynamics*, **57**, 455-467. https://doi.org/10.1007/s11071-008-9455-y

[6] Rahmani, M. and Behdinan, K. (2019) Investigation on the Effect of Coulomb Friction on Nose Landing Gear Shimmy. *Journal of Vibration and Control*, **25**, 255-272. https://doi.org/10.1177/1077546318774440

[7] Xiao, X.Z., Zhao, Y.Y., Wu, H. and Zhu, G.S. (2025) Dynamic Analysis of Nose Landing Gear Shimmy Considering Strut Height and Experiment on the Test Platform. *Open Journal of Applied Sciences*, **15**, 919-937. https://doi.org/10.4236/ojapps.2025.154062

[8] Sivakumar, S., Ganapathy Subramanian, L.R. and Giridharan, V. (2024) Shimmy Vibration Analysis of Unmanned Aircraft Coupled with Landing Gears. *Journal of Mechanical Science and Technology*, **38**, 137-147. https://doi.org/10.1007/s12206-023-1211-1

[9] Ruan, S., Zhang, M., Shi, X., Liu, X. and Nie, H. (2025) Stability Analysis of Shimmy under the Consideration of Tire Pavement Contact Mechanics Behavior. *Journal of Sound and Vibration*, **600**, Article ID: 118916. https://doi.org/10.1016/j.jsv.2024.118916